CORROSION SCIENCE AND TECHNOLOGY, Vol.31, No.6(2002), pp.476~484

Electrochemical Study on Localized Corrosion of Laser Surface Melted Alloy 600

Yun Soo Lim, Do Haeng Hur, Hong Pyo Kim, Joung Soo Kim, and Hyuk Sang Kwon*

Steam Generator Materials Project, Korea Atomic Energy Research Institute
P.O.Box 105, Yusong, Taejon 305-600, Korea.
**Department of Materials Science and Engineering, Korea Advanced Institute of Science and Technology*
373-1, Kusung-Dong, Yusong, Taejon, 305-701, Korea.

The effects of laser surface melting (LSM) on the resistance to localized corrosion such as intergranular stress corrosion cracking (IGSCC) and pitting of Ni-base Alloy 600 were investigated by electrochemical methods. The degree of sensitization of the laser treated Alloy 600 measured using the double loop electrochemical potentiokinetic reactivation method in a 0.1 M $Na_2S_4O_6$ + 20 ppm KSCN solution was considerably low, which demonstrates that the resistance to IGSCC of Alloy 600 in sulfur bearing environments was improved by LSM. The pitting potentials of Alloy 600 in 1 M NaCl at pH 4 and 9 were also markedly increased by the LSM process, compared with that of the non-laser treated Alloy 600. From the microscopic examination, it was found that pitting was initiated around sulfides associated TiN in the matrix of Alloy 600. Homogeneous microstructure associated with the reduction of inclusion size during LSM could be attributed to the increase of resistance to pitting corrosion in the LSM Alloy 600. On the other hand, complete dissolution of pre-existing intergranular Cr-rich carbides and the resultant Cr healing around grain boundaries was responsible for the improvement of IGSCC properties. The resistance to localized corrosion of the laser treated Alloy 600 was discussed from the results of the electrochemical test and microscopic examination.

Keywords : *Alloy 600, pitting corrosion, intergranular stress corrosion cracking, laser surface melting, electrochemical method*

1. Introduction

It is now well recognized that Ni-base Alloy 600, widely used as the steam generator tubing material in nuclear power plants, can suffer from various types of localized corrosion such as pitting, intergranular attack (IGA), and intergranular stress corrosion cracking (IGSCC) under pressurized water reactor operating conditions.[1] Although the mechanisms of the failure are not fully understood due to their complexity, it is generally accepted that grain boundary chemistry and microstructure are closely associated with the susceptibility to IGA/IGSCC.[2] In particular, the precipitation of Cr-rich carbides and the resultant creation of Cr depleted zones in the vicinity of the grain boundaries (commonly called 'sensitization') is known to play an important role in determining the alloy's susceptibility to IGA/IGSCC.[3] Once sensitized, Alloy 600 can suffer a vital intergranular fracture in the sulfur-bearing environments such as in sodium thiosulfate ($Na_2S_2O_3$) and sodium tetrathionate ($Na_2S_4O_6$) solutions even at low temperatures.[4] Pitting corrosion in Alloy 600 is known to be caused in chloride-containing and/or oxidizing environments.[5] The break down of passivating oxide films in aggressive environments is generally regarded as the mechanism of failure of this alloy. The inhomogeneities represented by nonmetallic inclusions locally reduce the stability of passive films, which consequently break down preferentially when exposed to aggressive environments, producing pitting corrosion. Recently Hur et al.[6] demonstrated that the pitting of Alloy 600 was initiated at the sites of sulfide inclusions physically associated with titanium nitrides. The role of a sulfide inclusion in stainless steels, as a site of pit initiation, has been well known over the past several decades.[7-12]

In previous studies, it was demonstrated that the resistance to IGSCC of the sensitized stainless steel[13] and the sensitized Alloy 600[14] in sulfur-bearing environments was improved by laser surface melting (LSM), mainly due to the metallurgical changes induced by the laser treatment.[15] During the failure by IGSCC, a crack starts at

the free surface and propagates through a connected pathway of the susceptible grain boundaries. Stewart and Williams[11] conducted LSM on type 304L stainless steels, and in their work LSM was shown to markedly improve the pitting resistance in neutral dilute chloride solutions. They found that LSM significantly reduced the size of sulfide inclusions, and concluded this was the most important effect of LSM leading to an improvement in pitting resistance.

The present work was aimed at investigating the effects of LSM on the intergranular and pitting corrosion properties of Alloy 600 by electrochemical methods. A double-loop electrochemical potentiokinetic reactivation (DL-EPR) test was conducted for the intergranular corrosion study in the sulfur-bearing environment, and the proper amount of KSCN was pre-determined before the DL-EPR test by examining the behavior of grain boundary attack in the sensitized Alloy 600. The measured degree of sensitization (DOS) under the well-established DL-EPR testing condition was analyzed in terms of the microstructural changes occurred by the LSM process. The pitting corrosion properties of Alloy 600 in chloride solutions were studied by potentiodynamic polarization tests. Finally, the effects of LSM on localized corrosion of Alloy 600 was evaluated and discussed from the experimental results.

2. Experimental

2.1 Specimen preparation

Mill annealed Alloy 600 plates 1.6 mm thick were used in this study, the alloy composition of which is shown in Table 1. The specimens were sealed in a quartz tube, solution annealed at 1050 ℃ for 30 minutes, and then water quenched (hereafter, referred to as SA Alloy 600, for short). Some of the SA Alloy 600 were subsequently sensitized at 600 ℃ for 24 hours and then followed by furnace cooling (hereafter, SA+SEN Alloy 600). A continuous CO_2 laser beam (maximum power of 4 kW) was used at a real laser power of 500 W, a beam diameter of 1 mm, and a scanning rate of 200 cm/min. (hereafter, LSM Alloy 600). Some of the LSM specimens were also subsequently sensitized under the same conditions as the SA+SEN Alloy 600 (hereafter, LSM+SEN Alloy 600). For observation with a scanning electron microscope (SEM), specimens were prepared by electrolytic etching in a solution of 2 % HCl + 98 % methanol at 6 V at room temperature.

Table 1. Chemical composition of the specimen used (wt%)

Ni	Cr	Fe	C	N	S	Si	Mn	Al	Ti	Nb	Mg
Bal.	15.9	7.6	0.04	0.04	0.002	0.15	0.17	0.12	0.21	tr.	0.008

2.2 DL-EPR test

Test solutions chosen for the evaluation of DOS were 0.01 M H_2SO_4, with varying the KSCN contents from 0 to 200 ppm. The test solutions were de-aerated by purging with purified N2 gas, before and during each DL-EPR test. The DL-EPR test was performed using a three-electrode cell system consisting of a saturated calomel electrode (SCE) as a reference, a platinum (Pt) electrode as a counter, and a specimen as a working electrode. The sample was kept immersed in the test solution for 0.5 - 1 hour at open-circuit. After attaining the stable corrosion potential (E_{corr}), the potential was raised in the anodic direction, from the value of E_{corr} to a potential in the passive range, at a scan rate of 0.5 mV/sec at room temperature. As soon as the pre-determined potential (600 mV_{SCE}) was reached, it was followed by a reactivation scan back to E_{corr} at the same scan rate. All the potentials were referred to a saturated calomel electrode (SCE).

2.3 Potentiodynamic polarization tests

1 M NaCl solutions at pH 4 and 10 were chosen for the investigation. The pH values were adjusted using HCl and NaOH. The test solutions were deaerated with nitrogen flow before and during each potentiodynamic polarization test. The apparatus for the potentiodynamic polarization tests were the same as in the case of the DL-EPT test. The sample was held at the corrosion potential for 2 hours to attain a stable value before polarization. After obtaining the stable corrosion potential (E_{corr}), the potential was raised in the anodic direction, from -100 mV below E_{corr}, at a scan rate of 0.5 mV/sec. The potentiodynamic polarization tests were carried out at temperatures of 30, 60 and 90 ℃, and repeated several times for each specimen to ensure reproducibility.

3. Results and discussion

3.1 Effects of the KSCN concentration on the DL-EPR test

Fig. 1(a), (b) show the DL-EPR curves for the SA Alloy 600, in 0.01 M H_2SO_4 solution without KSCN addition and with 5 ppm KSCN, and Fig. 1(c) shows the measured DOS from the SA Alloy 600 and the SA+SEN Alloy 600. DOS is defined as the percent ratio of the maximum current density in the reactivation loop (I_r) to that in the anodic loop (I_a), i.e., I_r / I_a x 100. It is evident from Fig. 1(a) and (b), that even the small addition of 5 ppm KSCN

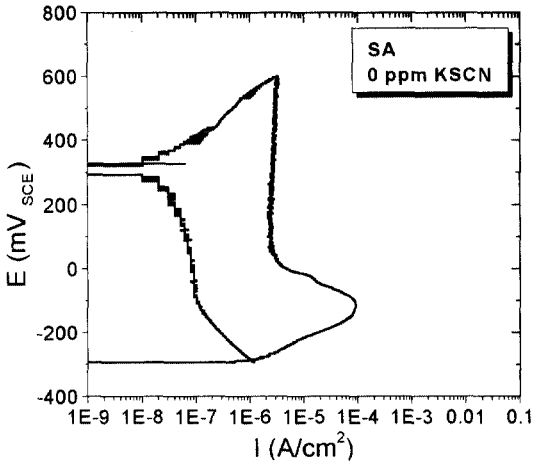

(a)

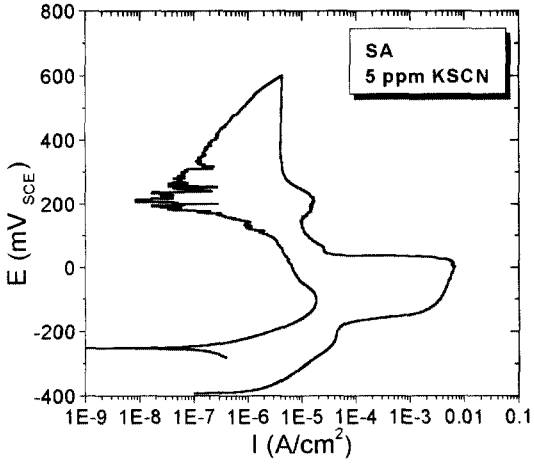

(b)

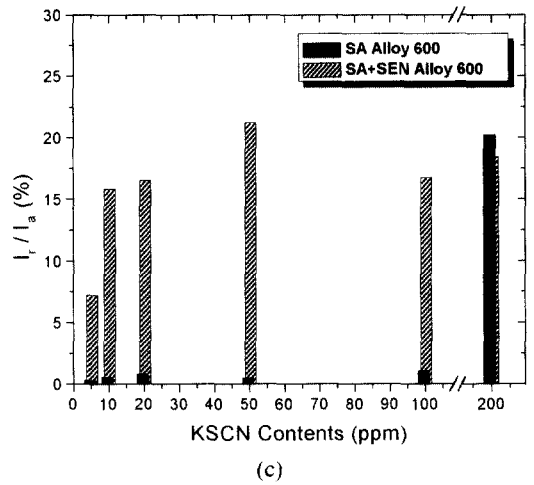

(c)

Fig. 1. DL-EPR curves for the SA Alloy 600 (a) without KSCN addition, (b) with 5 ppm KSCN, and (c) variations of the degree of sensitization as a function of the KSCN concentration for the SA Alloy 600 and SA+SEN Alloy 600, in 0.01 M H_2SO_4 solution at a scan rate of 0.5 mV/sec. at room temperature.

drastically increased the anodic current densities, i.e. from the order of 10^{-4} A/cm^2 to that of 10^{-2} A/cm^2. KSCN was, therefore, found to be a strong corrosive agent, as well as a grain boundary activator. With the KSCN concentration of 5 ppm, the DOS value from the SA+SEN Alloy 600 was only 7.18. On the other hand, at the KSCN concentration of 200 ppm, the DOS value from the SA+SEN Alloy 600 was lower than that from the SA Alloy 600, which seems to be unreasonable. The DOS values of the alloys were not considerably changed in the KSCN concentrations between 10 ppm and 100 ppm.

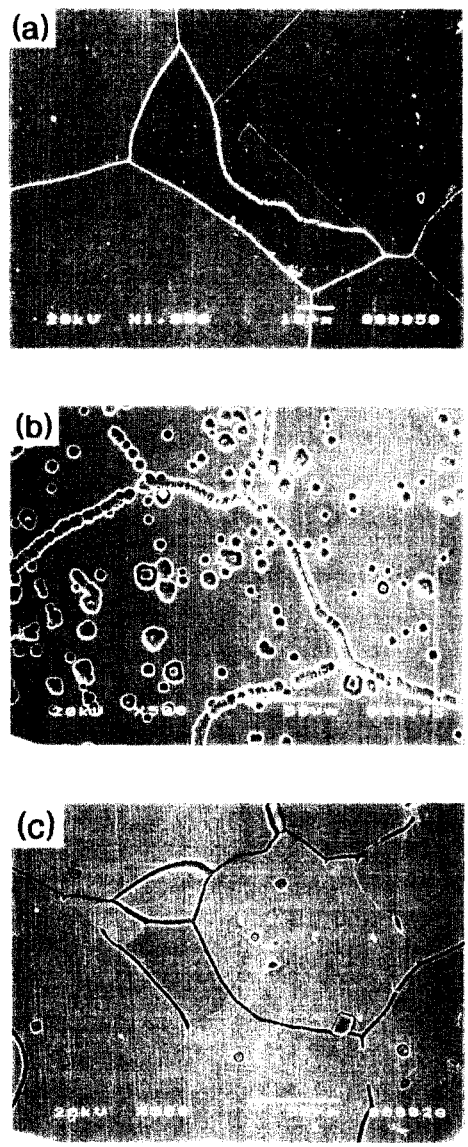

Fig. 2. SEM micrograph showing (a) intergranular Cr-rich carbides, and the grain boundary attacks with KSCN concentration of (b) 100 ppm, and (c) 20 ppm, in 0.01 M H_2SO_4 solution at a scan rate of 0.5 mV/sec at room temperature, obtained from the SA+SEN Alloy 600.

By the sensitization treatment, nearly continuous Cr-rich carbides were precipitated on most of the grain boundaries (Fig. 2(a)). The DOS values and the corroded surfaces from the DL-EPR test should, therefore, reflect the distribution morphology of Cr-rich carbides and the resultant Cr depletion along the grain boundaries to correctly evaluate the resistance to IGA/IGSCC of the alloy. Some of the grain boundary attacks in the SA+SEN Alloy 600 depending on the KSCN concentration from 5 ppm to 100 ppm were shown in Fig. 2(b) and 2(c). The grain boundaries became more severely attacked as the KSCN concentration increased. At the KSCN concentrations below 10 ppm, the grain boundaries were insufficiently attacked. When the KSCN concentration was 50 ppm, intragranular pitting was initiated, and when the KSCN concentration exceeded 100 ppm, severe pitting occurred within the grains (Fig. 2(b)). On the other hand, with 20 ppm KSCN addition, grain boundary attack was clearly revealed without any intergranular and intragranular pitting (Fig. 2(c)) and the measured DOS was relatively high (Fig. 1(c)). From the above results, it can be concluded that the proper amount of KSCN for selective grain boundary attack should be approximately 20 ppm under the present experimental conditions.

3.2 DL-EPR Results of the LSM and LSM+SEN Alloy 600

The DL-EPR curves from the LSM and the LSM+SEN specimens under optimized testing conditions were shown in Fig. 3(a) and (b). The first thing to notice is that the maximum current densities of the anodic loops in the Figures revealed similar values of approximately 10^{-2} A/cm^2. The results demonstrate that the general corrosion behavior of Alloy 600 was not changed by LSM. This is due primarily to the fact that no mass transfer occurred between the melt pool and the surrounding environment with sufficient Ar shielding during the LSM process. The average DOS values from the DL-EPR test are shown graphically in Fig. 3(c). The average DOS value from the LSM Alloy 600 was measured as 3.42, which was considerably lower than 16.5 of the SA+SEN Alloy 600. By the sensitization treatment, the DOS values of the LSM specimen increased due to the precipitation of grain boundary Cr-rich carbides. However, the extent of increase was not so large. The average DOS value from the LSM+SEN Alloy 600 was measured as 8.71, which was still much lower than that from the SA+SEN Alloy 600. From the above results, it can be concluded that the LSM Alloy 600 and the LSM+SEN Alloy 600 are more resistant to intergranular corrosion than the SA+SEN Alloy 600 in given corrosive environments.

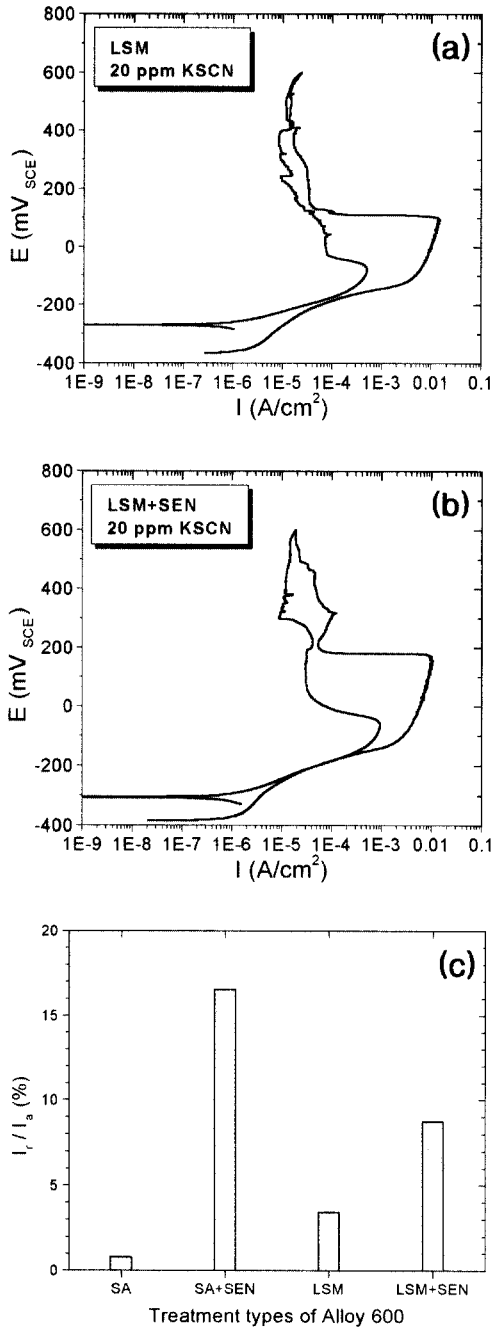

Fig. 3. DL-EPR curves from (a) the LSM Alloy 600, (b) the LSM+SEN Alloy 600, and (c) the degree of sensitization measured from the differently treated Alloy 600, in 0.01 M H_2SO_4 + 20 ppm KSCN at a scan rate of 0.5 mV/sec at room temperature.

Fig. 4(a) shows the particles formed in the laser melted zone during the LSM process. It shows that, no Cr-rich carbides are seen on the grain boundaries. This result originates from the fact that pre-existing Cr-rich carbides of the sensitized Alloy 600 were completely melted/dissolved due to the high energy density of a laser beam. Moreover, Cr-rich carbides were not re-precipitated during

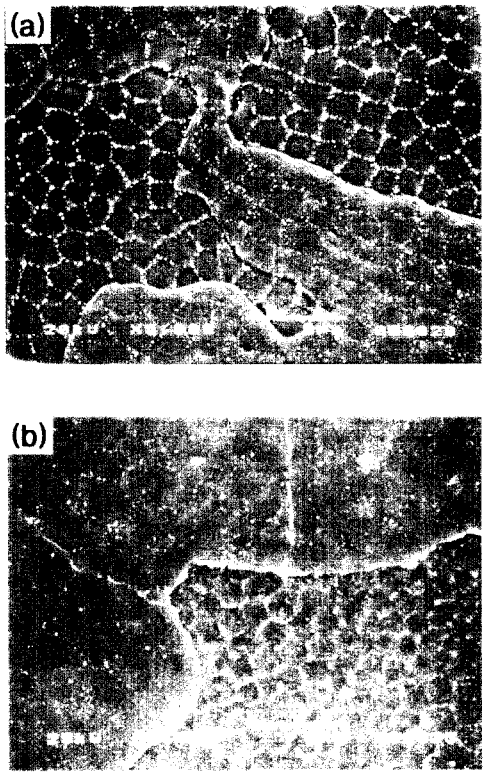

Fig. 4. SEM micrographs showing precipitates in the laser melted zone of (a) the LSM Alloy 600 and (b) the LSM+SEN Alloy 600, etched in a solution of 2 % HCl + 98 % methanol.

cooling due to the high cooling rate during the LSM process.[15] The microstructure of the LSM specimen, therefore, presumed to be equivalent to that of the SA specimen in the absence of grain boundary Cr-rich carbides. As a result, the low DOS value of the LSM Alloy 600 is caused by the de-sensitization (or, healing of the Cr depletion zones) due to the LSM process. The tiny particles along the cell boundaries were identified as TiN and MgS type particles by TEM analyses. Their formation can be attributed to the dissolution and subsequent re-precipitation of the pre-existing coarse particles in the commercial Alloy 600 during the LSM process.[15),16)]

The second phases in the LSM+SEN Alloy 600 are shown in Fig. 4(b). Compared with those in Fig. 4(a), there were no noticeable changes in the tiny particles, TiN and MgS type particles, along the cell boundaries within the grain by the sensitization treatment. Some Cr-rich carbides are seen on some grain boundaries in Fig. 4(b). They were identified as Cr-rich $M_{23}C_6$ and Cr_7C_3,[17] the same as in the case of the SA+SEN Alloy 600.[15] The average size of the Cr-rich carbides precipitated on the grain boundaries in the LSM+SEN Alloy 600 was much smaller than that in the SA+SEN Alloy 600. Moreover, they were sparsely distributed on the grain boundaries, and

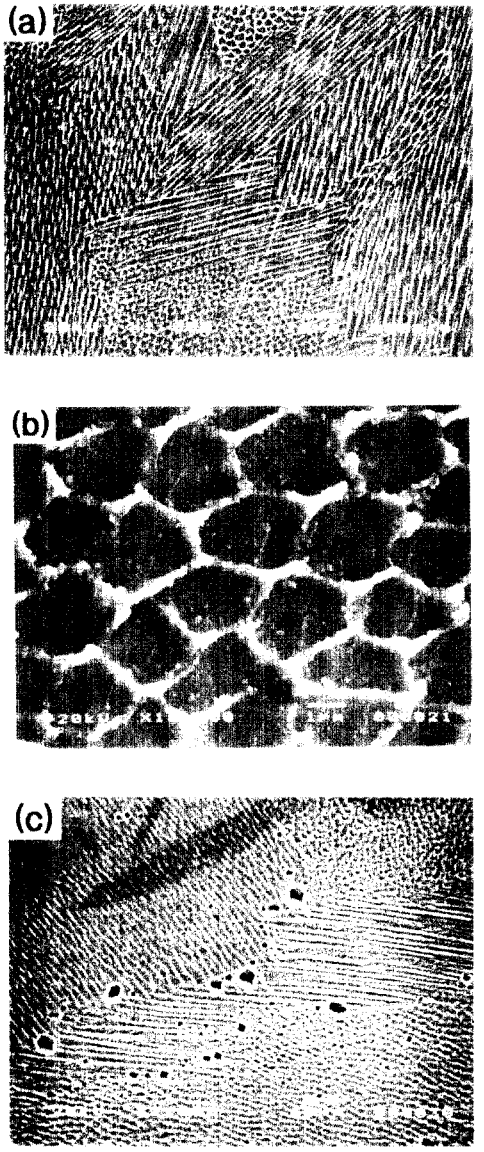

Fig. 5. SEM micrographs showing surface morphologies after DL-EPR test (a) for the LSM Alloy 600, (b) high magnified view of a part in (a), and (c) for the LSM+SEN Alloy 600, in 0.01 M H_2SO_4 + 20 ppm KSCN at a scan rate of 0.5 mV/sec at room temperature.

were found only on some high angle grain boundaries. The degree of Cr depletion on the grain boundaries was, therefore, not so severe. The minimum Cr concentration on the grain boundaries was measured as 12 wt%,[17] which was considerably higher than 7.3 wt% of the SA+SEN Alloy 600.[15] Therefore, it can be concluded that the laser treatment suppressed the precipitation of grain boundary Cr-rich carbides in Alloy 600, and this led to the low DOS value of the LSM+SEN Alloy 600, compared to that of the SA+SEN Alloy 600.

The grain boundary attacks in the LSM Alloy 600 and

the LSM+SEN Alloy 600 after the DL-EPR tests are shown in Fig. 5. The LSM Alloy 600 had no experience of grain boundary attacks, as shown in Fig. 5(a). The white contrast along the cell boundaries in Fig. 5(a) resulted from the different dissolution rate of the elements. Cr was more enriched along the cell boundaries due to the micro-segregation formed during the laser treatment.[15] Fig. 5(b) shows the high magnified view of a part in Fig. 5(a). The regions around the cell boundaries were more corrosion resistant due to the enriched Cr contents than those inside the cells in acidic solutions. Fig. 5(c) shows an image of the grain boundary attack in the LSM+SEN Alloy 600 with the KSCN concentrations of 20 ppm. As shown in the Figure, only some grain boundaries were discretely attacked, and the attacked morphology denotes exactly the distribution of grain boundary Cr-rich carbides (Fig. 4(b)).

3.3 Discussion on the DL-EPT results

The main advantages of the DL-EPR test to quantify the degree of susceptibility to IGA/IGSCC are that it is fast, quantitative, and reproducible. To correctly evaluate the susceptibility to IGA/IGSCC of Alloy 600, the DL-EPR test should be designed to attack only the Cr depleted regions, with other types of corrosion, such as pitting and general corrosion, suppressed. Roelandt and Vereecken[18] studied the test parameters on the evaluation of the susceptibility to intergranular corrosion of Alloy 600 by the SL-EPR test. They found that the appropriate concentration of KSCN should be below 10 ppm in 1 M H_2SO_4 at a scan rate of 2 V/h to cause only the selective grain boundary attack. In their study, however, pitting initiation could not be completely suppressed. Kruger et al.[19] claimed that 0.05 M KSCN should be used in 0.1 N H_2SO_4 at a scan rate of 1 mV/sec at room temperature to avoid intragranular pitting of the annealed Alloy 600. In the present study, the best results could be obtained with the electrolyte composition of 0.01 M H2SO4 + 20 ppm KSCN and a scan rate of 0.5 mV/sec at room temperature, which is a slight modification of the conditions suggested by Ahn et al.[20]

The average DOS value was considerably reduced (Fig. 3(c)), and grain boundary attack was not observed in the LSM Alloy 600 (Fig. 5(a)). From the microstructural examination, it was demonstrated that the microstructural changes of the grain boundaries in the sensitized Alloy 600 by the LSM process resulted in the improvement of the resistance to intergranular corrosion of the alloy. Suh et al.[14] studied the IGSCC resistance of the SA+SEN Alloy 600 and the LSM Alloy 600 through a slow strain rate test (SSRT) in neutral 0.1 M $Na_2S_4O_6$ solution at room temperature. They found that the fracture mode of the sensitized Alloy 600 was changed by LSM, i.e. from a brittle intergranular fracture of the SA+SEN Alloy 600 to a typical ductile transgranular failure of the LSM Alloy 600. Moreover, the stress corrosion cracks propagating from the free surface into the center of the sensitized specimen were arrested by the laser-melted track, making further propagation into the laser treated region impossible.[13),14] The present findings can, therefore, provide the electrochemical and microscopic evidence to their studies on the cause of improvement in the resistance to IGSCC of Alloy 600 in sulfur-bearing environments by the LSM process.

No continuous grain boundary attack was observed in the LSM+SEN Alloy 600 with the sufficiently reduced DOS value (Fig. 5(c) and Fig. 3(c)). Was et al.[21] correlated the degree of Cr depletion on the grain boundaries with the resistance to IGA of Alloy 600 by Heuy and Streicher tests. They found that severe IGA occurred when the measured Cr concentration on the grain boundary was below 9 wt% with a nearly continuous distribution of grain boundary Cr-rich carbides. Therefore, the LSM+SEN Alloy 600 should have a high resistance to IGA in acidic environments. Kai et al.[22] showed that the critical Cr concentration to prevent the IGSCC failure was around 8 wt% from the constant load test with the applied stress of 390 MPa, a pH of 3, and the $Na_2S_2O_3$ concentration of 0.001 M to 0.1 M at room temperature. Therefore, from the above studies by Suh et al.[14] and Kai et al.[22] in conjunction with the results of the DL-EPR test and microscopic examination in the present study, it can also be expected that the LSM+SEN Alloy 600 will have a high resistance to IGA/IGSCC in sulfur-bearing environments as well.

3.4 Potentiodynamic polarization test

Some of the potentiodynamic responses of the SA and LSM Alloy 600 in 1 M NaCl solution are shown in Fig. 6(a) at pH 4 at 90 ℃ and Fig. 6(b) at pH 10 at 60 ℃. By LSM, the corrosion potentials of the SA Alloy 600 were increased. However, the changes of corrosion rate in the passive regime were not significant. These results originate from the fact that the overall chemical composition of the LSM Alloy 600 was the same as that of the SA Alloy 600, since the laser beam was used only as a heat source. As a result, the general corrosion behaviors of Alloy 600 are hardly changed by the LSM process. This fact was also confirmed from the DL-EPR test in 0.01 M H_2SO_4 + 20 ppm KSCN solutions, as described before. The increase of pitting potential, as shown in the figures, was noticeable.

Fig. 7(a) presents the pitting potential changes of both

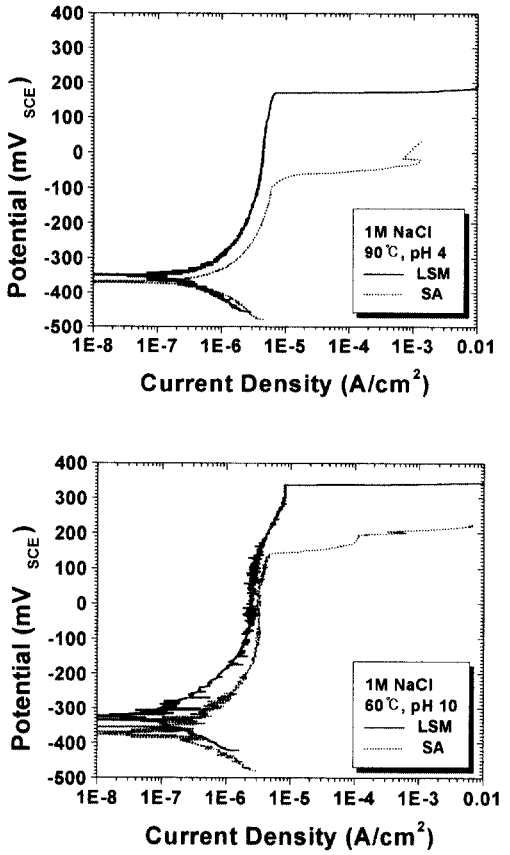

Fig. 6. Potentiodynamic polarization curves of the SA Alloy 600 and the LSM Alloy 600 in 1 M NaCl solution (a) at pH 4 at 90 ℃ and (b) at pH 10 at 60 ℃

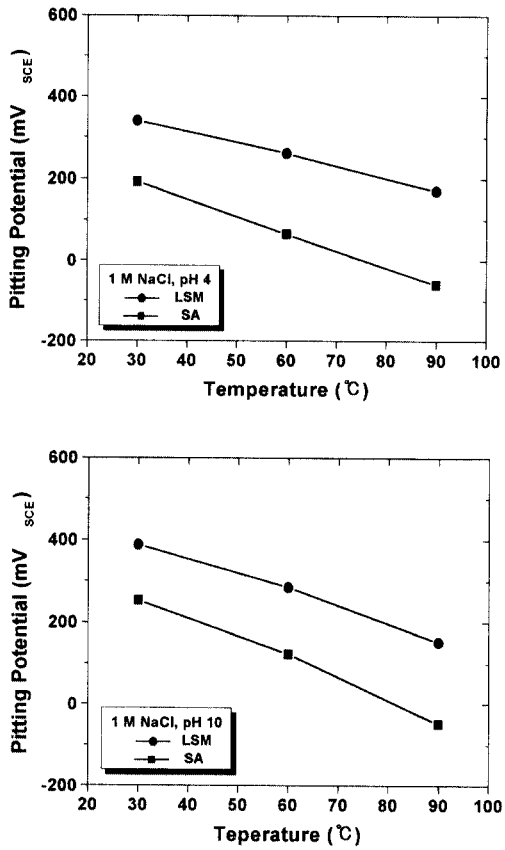

Fig. 7. Pitting potentials of the SA and LSM Alloy 600 as a function of temperature (a) at ph 4 and (b) at pH 10 in 1 M NaCl solution.

alloys depending on temperature in acidic solutions, and Fig. 7(b) in alkaline solutions. In any case, the pitting potential of Alloy 600 was increased 200 mV or higher by LSM. From these results, it is evident that the LSM process markedly improved the pitting resistance of Alloy 600 in chloride solutions. For a given alloy and temperature, the pitting potential in an acidic solution was a little lower than that in an alkaline solution. And the pitting potentials of both alloys seemed to decrease in a linear manner within the range of test temperature.

Fig. 8. shows the early stage of pit formation in the SA Alloy 600 after potentiodynamic polarization test. In this figure, the TiN inclusion itself did not dissolve, and corrosive attack was initiated at the periphery of TiN, making a micro-crevice

3.5 Discussion on the potentiodynamic polarization results

From the results of the potentiodynamic polarization test, the beneficial effect of LSM in the resistance to pitting corrosion of Alloy 600 was confirmed by a considerable increase in pitting potentials in corrosive environments.

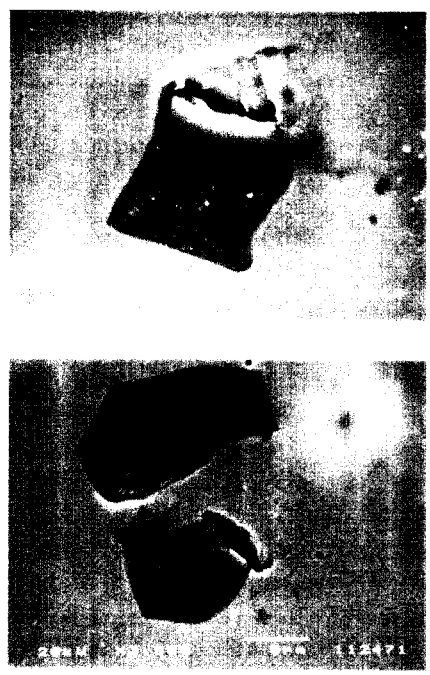

Fig. 8. SEM micrographs showing the early stage of pit initiation around TiN inclusion in SA Alloy 600.

The metallurgical changes induced by LSM should be responsible for the improvement in the pitting resistance of this alloy. The rapidly solidified microstructure by LSM is characterized by cellular dendrites with a small primary dendritic arm spacing of about 2 μm.[15] Lim et al.[15] reported that Cr was enriched on the cell boundaries by micro-segregation during solidification. However, the degree of Cr micro-segregation was not so large, an increase of approximate 2.6 wt%, due to fast cooling under the present LSM processing conditions. The important feature to be noticed, which can affect the pitting resistance of this alloy, will be the behaviors of inclusions during the LSM process. The pre-existing coarse inclusions before LSM, TiN and MgS (Fig. 8), were completely dissolved/melted by the high energy of a laser beam, and re-precipitated as tiny particles during solidification (Fig. 4(a)).

The nucleation sites of pits are frequently found to be related with the microscopic features of a metal surface. On stainless steels, for example, their location is usually found to be associated with sulfide inclusions, as was shown in the extensive works of Wraglen,[7] Eklund,[8] Castle and Ke,[9] and Baker and Castle.[10] The presence of MnS inclusions in stainless steels increases the susceptibility of the steel to pit formation. Using Scanning Auger electron microscopy, Baker and Castle[10] showed pits were always initiated at sites of Mn-enriched sulfides, irrespective of whether the sulfides were isolated or combined with some oxides. In stainless steels, sulfide inclusions are commonly found to be associated with oxides or nitrides. In that case, pit initiation can be even more facilitated since a deep microcrevice is formed at the periphery along the inclusion/matrix interface due to the preferential dissolution of the sulfide.

On Alloy 600, however, the mechanism on where and how the pits nucleate is not as well understood. An important observation made by several authors using SEM/EDS was a detection of strong sulfur peaks inside the propagating pits in spite of the very small amount (0.001 - 0.008 wt%) in the bulk before the corrosion test.[6),23] The solid solubility of sulfur in Ni is known to be extremely low; therefore, sulfur ions as impurities in the bulk are present mostly as sulfides of (calcium-substituted) MgS usually associated with titanium (carbo-) nitrides,[6] or segregated in the grain boundaries.[24] In the present study with SA Alloy 600, the corrosive attack was initiated at the TiN/matrix interface (Fig. 8). It is therefore suggested that, as in the case of stainless steels, the pitting of Alloy 600 can be initiated at the sites of sulfides attached TiN in Alloy 600. Hur et al.[6] studied the very inception of the pitting attack in Alloy 600. They also claimed that dissolution of sulfides attached to the TiN interface is the initial step in pit formation at these sites. Sulfide ions released by a corrosive attack on a sulfide inclusion spread out to the surrounding matrix surface[9] and accelerate (or activate) the anodic dissolution reaction.[25),26] Marcus et al.[26] investigated the influence of adsorbed sulfur on the electrochemical behaviors of the Ni-25Fe alloy in acidic solutions and showed that the presence of the monolayer of adsorbed sulfur enhances the dissolution rate and hinders the repassivation of base metal.

As well as playing the role of sulfide inclusions as preferred sites of pit initiation, it should be considered under what condition an incipient pit continuously propagates. The stable growth of a pit requires that the environment inside it be such that repassivation of the exposed base metal is inhibited. Stewart and Williams[11] investigated the effect of LSM on the resistance to pitting corrosion of commercial purity (0.011 wt% S) and high sulfur (0.080 wt% S) type 304 stainless steels. They found that LSM refined the size and reduced the visible volume fraction of sulfide inclusions in both alloys, resulting in the improvement of pitting resistance by reducing the pit nucleation frequency in the passive regime. From their results, they concluded that a sulfide inclusion should have a certain size at least (or critical size) to become a propagating pit. If the size of a sulfide is below the critical size, the underlying surface can easily be repassivated. Searson and Latanision[12] also reached the same conclusion with AISI 303 stainless steels that small and rounded sulfide inclusions resulted in small non-propagating pits while a few large sulfides produced more damaging pits.

4. Conclusions

1) The optimized DL-EPR testing condition for evaluating the degree of sensitization of Alloy 600 was established as the KSCN concentrations of 20 ppm in de-aerated 0.01 M H_2SO_4 solution with a scan rate of 0.5 mV/sec at room temperature. This optimized DL-EPR condition revealed the high DOS value for the sensitized Alloy 600 with suppression of other types of corrosion such as general and pitting corrosion.

2) LSM improved the resistance to intergranular corrosion of Alloy 600 by sufficiently reducing the average DOS value in acidic and sulfur-bearing environments. And the average DOS value of the LSM+SEN Alloy 600 was also much lower, compared with that of the SA+SEN Alloy 600. The different precipitation behaviors of intergranular Cr-rich carbides were responsible for the improvement of intergranular corrosion resistance of the laser

treated Alloy 600.

3) The pitting potentials of Alloy 600 were significantly increased by LSM in NaCl solutions. The improvement of pitting corrosion resistance can be attributed to the homogeneous microstructure and the refinement of non-metallic inclusions acting as potential sites for pit initiation.

4) Consequently, the LSM process was found to be an effective method for enhancing the resistance to localized corrosion in some corrosive environments.

References

1. T. U. Marston and R. L. Jones, in *Proc. 5th Int. Symp. on Environmental Degradation of Materials in Nuclear Power Systems - Water Reactors*, D. Cubicciotti, E.P. Simonen, R. Gold (Eds.), American Nuclear Society, Inc., La Grange Park, Illinois, 3 (1991).
2. G. S. Was, *Corrosion*, **46**, 319 (1990).
3. C. L. Briant, C. S. O'Toole, and E. L. Hall, *Corrosion*, **42**, 15 (1986).
4. R. C. Newman, R. Roberge, and R. Bandy, *Corrosion*, **39**, 386 (1983).
5. D. Choi and G. S. Was, *Corrosion*, **46**, 100 (1990).
6. D. H. Hur, W.C. Kim, U. C. Lee, and T. S. Park, *J. Corros. Sci. of Korea*, **27**, 43 (1998).
7. G. Wranglen, *Corros. Sci.*, **14**, 331 (1974).
8. G. S. Eklund, *J. Electrochem. Soc.*, **121**, 467 (1974).
9. J. E. Castle and R. Ke, *Corros. Sci.*, **30**, 409 (1990).
10. M. A. Baker and J.E. Castle, *Corros. Sci.*, **34**, 667 (1993).
11. J. Stewart and D.E. Williams, *Corros. Sci.*, **33**, 457 (1992).
12. P. C. Searson and R.M. Latanision, *Corrosion*, **42**, 161 (1986).
13. J. Stewart, D. B. Wells, P.M. Scott, and A.S. Bransden. *Corrosion*, **46**, 618 (1990).
14. J. H. Suh, J. K. Shin, S.-J. L. Kang, Y. S. Lim, I. H. Kuk, and J. S. Kim, *Mater. Sci. Eng. A*, **A254**, 67 (1998).
15. Y. S. Lim, J. H. Suh, I. H. Kuk, and J. S. Kim, *Metall. Trans. A*, **28A**, 1223 (1997).
16. Y. S. Lim, J. S. Kim, and H. S. Kwon, *Metall. Trans. A*, **32A**, 1248 (2001).
17. Y. S. Lim, J. S. Kim, and H. S. Kwon, *Mater. Sci. Eng. A*, **A279**, 192 (2000).
18. A. Roelandt and J. Vereecken, *Corrosion*, **42**, 289 (1986).
19. R. M. Kruger, S. F. Claeys, and G. S. Was, *Corrosion*, **41**, 504 (1985).
20. M. K. Ahn, H. S. Kwon, and J. H. Lee, *Corrosion*, **51**, 441 (1995).
21. G. S. Was, H. H. Tischner, and R. M. Latanision, *Metall. Trans. A*, **12A**, 1397 (1981).
22. J. J. Kai, C. H. Tsai, T. A. Huang, and M. N. Liu, *Metall. Trans. A*, **20A**, 1077 (1989).
23. C. B. In, Y. I. Kim, W. W. Kim, J. S. Kim, S. S. Chun, and W.J. Lee, *J. Nucl. Mater.*, **224**, 71 (1995).
24. R. M Latanision and M. Kurkela, *Corrosion*, **39**, 174 (1983).
25. J. Oudar, *Br. Corros. J.*, **25**, 21 (1990).
26. P. Marcus, A. Teissier, and J. Oudar, *Corros. Sci.*, **24**, 259 (1984).